Applied Thermal Engineering 88 (2015) 33–46

Contents lists available at ScienceDirect

Applied Thermal Engineering

journal homepage: www.elsevier.com/locate/apthermeng

Research paper

Fluid dynamic and heat transfer processes between solid surfaces and non-Newtonian liquid droplets

A.S. Moita*, D. Herrmann, A.L.N. Moreira

IN+ - Center for Innovation, Technology and Policy Research, Instituto Superior Técnico, Universidade de Lisboa, Portugal

HIGHLIGHTS

- Dynamics and heat transfer are described for the impact of shear-thinning droplets.
- Without boiling, the shear-thinning effect is governed by the gum concentration.
- An alternative model to predict the spreading diameter is proposed.
- Thermal induced atomization is weakly dependent on the non-Newtonian viscosity.

ARTICLE INFO

Article history:
Received 20 June 2014
Received in revised form
20 October 2014
Accepted 15 November 2014
Available online 25 November 2014

Keywords:
Non-Newtonian droplets
Heated surfaces
Spreading model
Phase Doppler measurements
Cooling effectiveness
Thermal induced atomization

ABSTRACT

This paper addresses the experimental and theoretical description of the fluid dynamic and thermal behaviour of non-Newtonian (shear-thinning) droplets impacting onto smooth and micro-patterned heated surfaces. The shear-thinning liquids are mixtures of water + xanthan gum prepared with different concentrations of the gum, namely 0.05%, 0.10%, 0.15% and 0.35%wt. For droplet impacts over the surfaces heated bellow the boiling temperature of the liquid, the shear-thinning effect is clearly governed by the concentration of the non-Newtonian component, which is associated to the consistency coefficient of the constitutive model describing the viscous behaviour of the flow. In line with this, models predicting the spreading of Newtonian droplets are revisited and an alternative one is proposed, which integrates the non-Newtonian behaviour. The results suggest that heating the surface (and consequently the liquid) alters the rheology of the non-Newtonian mixture and reverses the increase of the zero viscosity, which is observed for impacts onto non-heated surfaces, thus allowing a larger spreading diameter and a significant recoiling phase for droplets with high concentrations of the non-Newtonian component. The heat transferred at droplet–surface interaction, during the spreading of the droplet is also evaluated. The analysis evidences the strong coupling between the heat transfer process and the spreading dynamics, for the non-Newtonian droplets. Further heating the surface above the boiling temperature of the liquid, the droplets impact the surfaces within the nucleate boiling regime and thermal induced atomization occurs. In this case, Phase Doppler measurements are taken to characterize the size of the secondary droplets generated within this process. The results show that the thermal induced atomization is mainly triggered by the force balance between surface tension and vapour pressure forces, so the viscosity plays a secondary role.

1. Introduction

Unlike Newtonian fluids, for which the stress tensor is a linear function of the velocity gradient and therefore the viscosity remains constant, regardless of the shear rate, in non-Newtonian fluids, the stress tensor is a generic function of the velocity gradient and of its derivatives. Usually, non-Newtonian fluids are categorized in three main groups: i) power-law (or Ostwald-De Waele) fluids, ii) yield-stress fluids and iii) viscoelastic fluids. Power law fluids are the simplest type of non-Newtonian fluids, for which the viscosity μ is simply related to the shear rate $\dot{\gamma}$ by the so-called Ostwald-De Waele equation:

* Corresponding author. IN+ – Center for Innovation, Technology and Policy Research, Instituto Superior Técnico, Universidade de Lisboa, Av. Rovisco Pais, 1049-001 Lisboa, Portugal. Tel.: +351 21 841 7876; fax: +351 21 849 6156.
E-mail address: anamoita@dem.ist.utl.pt (A.S. Moita).

http://dx.doi.org/10.1016/j.applthermaleng.2014.11.042
1359-4311/

$$\mu = K\dot{\gamma}^{n-1} \quad (1)$$

Here K and n are constants of empirical nature. K is called as consistency coefficient and describes the fluid viscosity at low shear rates and matches with the Newtonian viscosity for $n = 0$. The power-law index n determines the behaviour of the fluid. Hence, the fluids are shear-thinning when $n < 1$ (i.e. the viscosity decreases with the shear rate) and shear thickening for $n > 1$. From the physico–chemical point of view, the shear thinning behaviour can be explained by the breakdown of the structure formed by interacting particles within the fluid, while the shear-thickening is often related to flow-induced jamming [1,2].

Viscoplastic (or yield-stress) fluids only flow when the applied stresses overcome a critical value (the yield stress). For applied stresses lower than the yield stress, these fluids behave like elastic solids. The simplest constitutive model describing the viscous behaviour of these fluids was proposed by Bingham [3] and introduces the shear stress component as a linear function of the velocity gradient. This intercepts at a critical value τ_c corresponding to the threshold yield point. Further improvements to the Bingham model were later proposed by Herschel–Bulkley [4] and by Papanastasiou [5]. The definition of yield-stress behaviour for a fluid instead of a solid is still a topic for discussion nowadays. More extensive reviews on this subject can be found for instance in Refs. [6–8].

Finally, in viscoelastic fluids (*e.g.* several polymer melts or solutions), part of the deformation energy is stored and released later, being the delay between energy storage and release related to a relaxation time. The main characteristic of this group of non-Newtonian fluids is the occurrence of elastic stress effects, for sufficiently high shear rates. This characteristic leads to an anisotropic application of the normal forces (*e.g.* pressure) acting on liquid finite element, contrarily to what occurs in Newtonian fluids. Pioneering work introduced by Maxwell provides the basic constitutive model for linear viscoelastic fluids. A more elaborate model and probably the most popular is the Oldroyd-B model [6–9]. More recent constitutive models have been proposed for instance by Zhu et al. [10] to describe flow induced anisotropic behaviour of viscoelastic fluids.

Non-Newtonian fluid flows are present in a variety of situations. Droplet–wall interactions are a particularly interesting flow given its interest in numerous applications, such as coating, painting or printing (*e.g.* Refs. [11–13]). Also, droplet–wall interactions involving non-Newtonian fluids are an interesting problem, from the phenomenological point of view, since they involve large spatial and temporal gradients, which will strongly alter the viscous behaviour. However, despite all the aforementioned arguments, non-Newtonian flows are studied for several decades (*e.g.* Refs. [14,15]) and droplet–wall interactions of Newtonian fluids are investigated for over a century, but the study of non-Newtonian droplets impacting onto rigid surfaces is still sparsely reported in the literature. The spreading of yield-stress (polymer) droplets over non-heated surfaces was investigated by several authors. From the various conclusions withdrawn in these studies, it is worth noting that the maximum spreading diameter decreases linearly with the yield stress magnitude (*e.g.* Refs. [16–19]). This contrasts with the power law dependence of the spreading diameter with the liquid viscosity that is usually reported for Newtonian droplets [20,21]. Most of these studies were performed for impacts onto cold and smooth surfaces. Exception is made to the work of Saidi et al. [22] who attempted to quantify the effect of the surface topography and wettability on the dynamic behaviour of yield-stress droplets. The authors also tried to determine the effect of apparent wall slip, but the results obtained were inconclusive since, as well pointed by Bertola and Marengo [2] it is impossible to distinguish between the two effects in the experiments performed by Saidi et al. [22]. Nevertheless, the results suggest a weak dependence of the maximum spreading diameter on surface wettability. The research performed on the impact of viscoelastic droplets also focus on the spreading over non-heated surfaces [23]. Some analysis of the disintegration of viscoelastic droplets was also performed in Refs. [24], but this is mainly the result of the impact onto a very small target. Most of the experimental results are also consistent in the fact that the addition of a viscoelastic component tends to preclude the occurrence of droplet rebound and/or disintegration [25], due to the strong dissipative effect occurring at the contact line.

An increasingly interest on droplet–wall interactions of non-Newtonian liquids and particularly of shear-thinning droplets is related to their relevance in various biological applications. For instance, droplet impacts of non-Newtonian preparations are the basic working principle of a method called cell printing. In this method various techniques similar to inkjet are being used to deploy living cells on a substrate to create tissue, neural cells and possibly organs (*e.g.* Refs. [26,27]). In this case, great care is necessary as the cells are extremely sensitive to shear stresses and can be easily destroyed as the droplet impacts and spreads over the surface. Similar disruptive effects have been reported in the transport of DNA samples for several years (*e.g.* Ref. [28]). Blood is a shear-thinning fluid whose behaviour is well characterized by eq. (1). Modifications of the values of the consistency coefficient K and of the power-law index n are suggested to be correlated with leukaemia [29,30].

In this context, few studies have addressed the spreading behaviour of shear-thinning droplets over smooth and cold surfaces. German and Bertola [17] and later An and Lee [31] report a significant decrease in the viscosity during spreading, which leads to a wider spreading diameter for the shear-thinning droplets, at the earlier stages after spreading. Nevertheless, the spreading diameter is generally lower for the shear thinning fluids, as a result of the higher value of the zero viscosity. German and Bertola [17] tried to relate this behaviour with the consistency coefficient K and with the power law exponent n. Their conclusions are limited to the fact that it is very difficult to change K independently from n. Nevertheless, their results suggest a dominant effect of K in the spreading, which was related to an increase of the concentration of the shear-thinning component. Based on their experimental data, An and Lee [32] adapted correlations existing in the literature to predict the spreading diameter of Newtonian droplets (devised from energy conservation principles) to their shear-thinning droplets. This adjustment was based on empirical fitting of the data combined with a re-scaling of the viscous dissipative term. Despite the modified relations reported by An and Lee [32] are well adjusted to their experimental data, they have a strong empirical nature.

Almost any information is found in the literature concerning impacts over heated and/or over rough surfaces.

Extensive investigation has been developed on droplet impacts onto heated surfaces within the various boiling regimes. The definition of the boiling regimes following the Nukyiama curve is itself a matter of investigation as it depends on the properties of the entire system, including those of the surface as, for instance surface topography, as well as on the dynamic (impact) conditions. This is particularly relevant in determining the Leidenfrost temperature, as revised for instance by Bernardin and Mudawar [33]. Hence, the heat transfer regimes for an impacting droplet are qualitatively similar to those defined in the Nukyiama curve, but significant deviations can be quantitatively observed. Numerous studies describe the morphological characteristics of the impinging droplets, many of them focussing on the spreading within the film

evaporation regime and rebound within the film boiling regime (*e.g.* Refs. [34–40]).

Describing the heat transfer during droplet impact and spreading is quite a complex task. To simplify it, many authors consider that the temperature at the liquid–surface interface is constant and the heat flux from the surface to the lamella is assumed to be initially uniform. Such assumption only holds for high thermal conductivity surface materials [41–43]. More recently, in the attempt to verify the assumptions of the temperature variation at droplet–wall interactions, measurements of the surface temperature have been reported both for sessile, *e.g.* Ref. [43] and impacting drops [45–49]. Theoretical models of liquid vaporization and prediction of liquid and surface temperatures were also proposed by few authors, many of them considering a constant and uniform liquid–solid interface temperature [50–53]. A slightly different approach is followed by Refs. [49], although in this case, the study was mainly focused on predicting the heat flux.

Despite these valuable efforts, which allowed significant progress in the description of the heat transfer at droplet–surface interactions, a full consensual description has not yet been achieved. Also, many issues must still be overcome, such as the accurate description of the contact temperature, obtained at liquid–solid interface, which takes into account the heterogeneities of temperature distribution during the spreading motion. In this context, Moita et al. [54] proposed a new approach for the theoretical analysis of the flow and the temperature fields in a spreading droplet and in the solid substrate, based on a similarity solution of the Navier–Stokes equations, coupled with the energy equation. The solution accounts for the variation of the thermal properties of the liquids with the temperature, which have been shown by Healy et al. [35] to be of major importance. One of the limitations of the model of Moita et al. [54] is the fact that it mainly focus on the heat transfer occurring at the earlier stages after impact (for a difference in the dimensionless times $t^* - t_0^* < 5$, with $t^* = tU_0/D_0$ represents the instant of impact). As it will be further discussed in the results, an important part of the heat transfer between the droplet and the surface occurs indeed during this period. However, as experimentally and theoretically described for instance by Pasandideh–Fard et al. [47], the heat transfer process is affected by the spreading area, and therefore, the later stages of spreading and even the recoiling phases should not be neglected.

Another limitation of the model of Moita et al. [54] is the fact that it does not account for the effect of surface topography. It is known, from the impact of Newtonian droplets that the modification of surface topography and/or wettability strongly affects droplet dynamics (*e.g.* Ref. [55]). Hence, several authors have developed new techniques to alter the surface wettability and topography in a custom made and well controlled manner (*e.g.* Refs. [56–60]). However, very little work is done on the description of the heat transfer processes over heated and modified surfaces, exception made for instance to Weickgenannt et al. [61] and to Moita and Moreira [62]. Such research is practically inexistent when dealing with non-Newtonian droplets. In line with this, the present paper focuses on the fluid dynamic and heat transfer processes occurring between non-Newtonian (shear-thinning) droplets and solid surfaces. In the context of the aforementioned applications, major focus is put on the spreading (and receding) behaviour, although the thermal induced atomization, generated when the surface is heated above the saturation temperature of the fluids, must also be discussed. Hence, the analysis will be divided in three main parts. The first concerns the experimental description of the spreading behaviour of shear-thinning droplets over cold and heated surfaces and will discuss the influence of several parameters, including those relevant to the accurate devise of the viscosity constitutive model. Surface wettability and topography are also investigated for surfaces heated up to the boiling temperature (to avoid the occurrence of thermal induced atomization). Based on this analysis, an alternative relation is proposed here to predict the spreading of the shear-thinning droplets, which is compared with data reported in the literature and with our own experimental results. Afterwards, the heat transfer processes occurring during the interaction between the droplet and the surface are also discussed. Such analysis is performed after a detailed description of the spreading behaviour, since, following the bibliographic review made so far, the heat transfer process is known to depend on the spreading mechanism.

Finally, the surface is heated above the boiling temperature of the fluid and secondary (thermal induced) atomization occurs, which will be characterized for impacts onto smooth surfaces, in terms of size of the ejected secondary droplets. Despite thermal induced atomization is an unwanted phenomenon for most of the applications referred in this Introduction, it must be characterized in order to be controlled. For instance, Bertola and Sefiane [63] suggest that the thermal induced atomization can be controlled in viscoelastic droplets by adding a viscoelastic polymer, but their analysis is mostly qualitative and based on visualization, so either the size or the velocity of the secondary droplets is investigated.

2. Experimental set-up and procedures

The experiments encompass the impact of droplets on solid and dry surfaces, with velocities U_0 ranging from 0.8 to 4 m/s. The initial droplets' diameter is fixed ($D_0 = 3.2$ mm).

The surfaces are accommodated on a copper base in which a 264 W cartridge heater is inserted and are heated from room temperatures up to 140 °C. Surface temperature of the targets is acquired using fast response type K thermocouples “Medtherm”. The thermocouples are 3 mm apart, taking from the reference the thermocouple that is placed in the center of the droplet impact region ($r = 0$ mm). They are aligned with the top of the surface where the impact occurs. Another embedded thermocouple is used to control the cartridge heaters, using a PMA KS20-I controller. The signal of the thermocouples is sampled with a National Instruments DAQ board plus a BNC2120 and amplified with a gain of 300 before processing. Different acquisition frequencies were used to characterize the temporal variation of the instantaneous temperature. To be able to capture the temperature variation along the whole spreading process of the lamella, a relatively small acquisition frequency must be used (of the order of 2 kHz). Then, for each impact condition, the measures taken at the instants right after impact are further refined using a larger acquisition frequency, of the order of 10 kHz. Comprehensive description of the set-up can be found, for instance in Moita and Moreira [62].

Care is taken to assure that the surface is dry and recovers the initial temperature before the impact of the droplet. The liquid is kept at the droplet generator at room temperature and atmospheric pressure. Ambient temperature and relative humidity were measured through the experiments to ensure that their variation did not produce relevant changes in the results.

Droplet impacts are recorded using a high-speed camera (Phantom v4.2 from Vision Research Inc., with 512 × 512pixels@2100 fps and a maximum frame rate of 90 kfps). To record the impact history of the millimetric droplets, the frame rate was set to 2200 fps. For this set-up, the resolution is 25 pixel/μm. The spreading diameter is evaluated based on a home-made post-processing routine developed in Matlab®. The spreading curves are averaged over 6 impact events, obtained at similar experimental conditions.

Besides water, which was used as the control fluid, the experiments were performed with shear-thinning mixtures of water with

xanthan gum (wt%). The viscosity vs shear rate curves were fitted using the Cross model [64]:

$$\frac{\eta_{\text{eff}} - \eta_\infty}{\eta_0 - \eta_\infty} = \frac{1}{1 + (C\dot{\gamma})^m} \quad (2)$$

being η_{eff}, η_0 and η_∞ the effective, zero-shear (upper limit) and infinite-shear (lower limit) viscosities, respectively. C is the Cross time constant and $m = 1-n$. Thus, as m increases, the mixture becomes more shear-thinning.

The fitting parameters are given in Table 1, which summarizes the main physico–chemical properties of the fluids, taken at ambient temperature and pressure. The rheological data was measured at controlled temperature conditions, at ATS RheoSystems (a division of CANNON® Instruments, Co). The accuracy of the data is within ±5%. In the table, X stands for xanthan and the percentage following is the wt% of xanthan gum in the mixture with water. It is worth mentioning that except for the viscosity, all the other properties of the xanthan gum solutions are very close to those of water.

As for other relevant thermal properties, any significant difference was detected between water and the water + xanthan gum mixtures. Hence, one may consider that for all the mixtures, the saturation temperature (at ambient pressure) is 100 °C, the thermal conductivity is 607 × 10^{-3} $WK^{-1}m^{-1}$, the specific heat is 4.18 $kJkg^{-1}K^{-1}$ and the latent heat of vaporization is 2272 $kJkg^{-1}$.

2.1. Characterization of the surfaces

Besides the smooth silicon wafer surface, which was used for the majority of the experiments, 2 surfaces micro-structured with regular patterns and 1 hydrophobic surface micro-structured with stochastic patterns were used. To prepare the surfaces with regular patterns, the wafer is coated with aluminium (to allow a deeper etching) and afterwards with photoresist. The regular patterns are transferred by high resolution printing (performed at INESC-MN) and photolithography and are then submitted to plasma etching for 5–7 h. This procedure assures the anisotropic etching to create the required dimensions of the micro-patterns. Finally, wet etching is used to remove the aluminium coating. These patterns are composed by square pillars of size a, height h_R and pitch λ. Fig. 1 defines schematically these quantities.

The surface with stochastic profiles is prepared using a grafting technique. The roughness profiles of all the surfaces were measured using a Dektak 3 profile metre (Veeco) with a vertical resolution of 200 Å. For the stochastic profiles, roughness amplitude must be quantified by average values. Following the procedures recommended by most of the previous studies on droplet/wall interactions [65–67] the roughness amplitude of these surfaces was quantified by the mean roughness R_a (according to standard BS1134) and by the average peak-to-valley height R_z (according to standard DIN 4768).

Wettability was also characterized, being quantified by the static contact angle θ, using an optical tensiometer THETA from Attension,

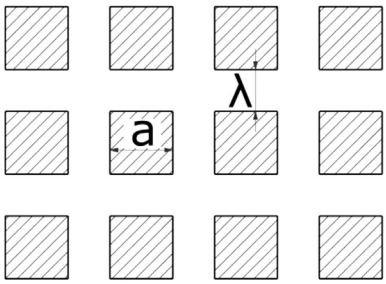

Fig. 1. Schematic showing the definition of the dimensions a and λ characterizing the topography of the surfaces micro-structured with regular patterns.

with One-Attension v1.8 software. An average value is considered for each pair liquid-surface which is determined from at least five measurements taken at different regions of the surface. The time evolution of the average contact angles is obtained by curve fitting and the final values are determined by extrapolation. The measurements were performed at room temperature.

Hysteresis was also taken for the surface with the highest contact angle, to verify that it was superhydrophobic. According for instance to Bhushan and Jung [68], for a surface to be superhydrophobic the equilibrium angle must be higher than 150°, but the contact angle hysteresis must be lower than 10°. The hysteresis measured for the surface with the highest contact angle was 8°, so it can be considered superhydrophobic. None of the other surfaces satisfies the conditions for superhydrophobicity.

Regarding the wetting behaviour of the surfaces, a basic analysis was performed only to assess whether the wetting state was closer to that of Wenzel or to that of Cassie and Baxter regimes. All the theoretical angles predicted by the Wenzel regime are significantly closer to those measured experimentally. Except for the superhydrophobic surface, even when the contact angles are close to 100°, a stable Cassie and Baxter state was not observed and the droplet could easily penetrate through the pillars. This was detected, during the measurement of the contact angles, by visual inspection of the droplets in contact with the surfaces with the optical microscope, coupled to the CCD camera, in the optic tensiometer. Details on the characterization of the wetting behaviour can be found, for instance in Refs. [62,66].

Table 2 summarizes the topographical and wetting properties of the working surfaces. Regarding the thermo-physical properties of the silicon wafer, the thermal conductivity is 149 $WK^{-1}m^{-1}$, the specific heat is 0.7 $Jg^{-1}K^{-1}$ and the density is 2329 kgm^{-3}.

2.2. Characterization of the thermal induced atomization

Phase Doppler measurements were performed using a two-component system from Dantec. The optical configuration is summarized in Table 3. The measurement grid uses a radial system, as defined in Fig. 2, where $r = 0$ mm corresponds to the center of the impact region. Here, U and V stand, as usual, for the axial and radial velocity components, respectively. Positive values of the axial

Table 1
Thermophysical properties of the working fluids taken at 20 °C. Here X stands for xanthan and the percentage following is the wt% of xanthan gum in the mixture with water.

Fluid	ρ [kg/m^3]	σ_{lv} [N/m] × 10^3	η_0 [Pa·s]	η_∞ [Pa·s]	C [s]	m [−]
Water	996	72.75	8.9 × 10^{-4}	8.9 × 10^{-4}	–	–
X0.05%	997	73.00	0.08	1.9	0.8	0.678
X0.10%	997	72.00	0.22	2.6	1.3	0.696
X0.15%	997	71.50	0.58	3.6	1.65	0.707
X0.35%	997	72.95	13.29	5.1	13.97	0.804

Table 2
Surface topography and wettability with water of the surfaces used in the present study. Here a is the size of the side of the squares, h_R is the height of the squared pillars and λ is the pitch.

Surfaces	a [μm]	h_R [μm]	λ [μm]	R_a [μm]	R_z [μm]	θ [°]
Smooth	–	–	–	~0	~0	76.1 ± 4
Structured w/regular	282	7.6	342	–	–	84.9 ± 4
patterns	161.6	23.1	396.9	–	–	96.3 ± 4
Structured w/stochastic profile	–	–	–	4.19	8.0	154.3 ± 2

velocity U are taken downwards, in the direction of gravity, the same as for the impact velocity of the primary droplet U_0.

Measurements are reported at $z = 5$ mm, above the surface and at radial coordinates $r = 0$ mm, $r = 3$ mm and $r = 6$ mm. These coordinates were selected based on previous work (*e.g.* Moita and Moreira [62]).

Temperature variation of the refractive index n of water, was estimated for the range up to the boiling temperature of the liquids, as in Dreisbach [69] or Pitcher et al. [70], by making use of the Eykman formula $(n^2 - 1)/(n + 0.4) = A\rho$, where A is a fitting constant [71]. Despite the scattering angle used here is not the one reducing to the minimum the influence of the refractive index in the measures, inaccuracy of the size measurements is still better than 7%. Regarding the refractive indexes of the water + xanthan mixtures, the values were taken by interpolation, following the study of Basavaraju et al. [72].

To obtain statistically representative measurements, ten thousand valid samples were considered for each impact condition. This number results from a discrete probability distribution assessment as in Refs. [73,74].

2.3. Measurement uncertainties and inaccuracies

In terms of measurement inaccuracies and uncertainties, the uncertainty of the temperature measurements is determined as in Ref. [75] is ±1.2 °C.

The accuracy in the determination of the droplets' initial diameter D_0, statistically determined from 50 impacts is ±1.4%, while the accuracy in the evaluation of the impact velocity U_0 is better than 3%. Accuracy of the measurements of the spreading diameter from image processing is evaluated to be ±25 μm.

The accuracy in the determination of the rheological data is within ±5%.

Regarding the characterization of the surfaces, the topographical profiles are evaluated within an accuracy of ±200 Å. The uncertainty of the measurements for the contact angles is provided in Table 2.

Finally, the evaluation of the errors and inaccuracies of the phase Doppler measurements is not trivial, as summarized in sub-Section 2.2. The highest uncertainty is associated to the evaluation of the refractive index under the particularly demanding experimental conditions used here, which was evaluated as in Pitcher et al. [70] to be of the order of 7%. Detailed evaluation of the sources of errors and inaccuracies for the phase Doppler measurements is reported in Moita and Moreira [71].

3. Results and discussion

3.1. Spreading of shear-thinning droplets

The morphology of shear-thinning droplets spreading onto smooth and cold surfaces is quite similar to that of Newtonian droplets (*e.g.* water). Quantitative differences are however evidenced, which are associated with the non-linear viscous dissipation occurring at acceleration and deceleration of the fluid during spreading and receding. A direct comparison, as shown in Fig. 3 emphasizes the main differences between Newtonian and non-Newtonian fluids.

Table 3
Outline of the phase Doppler optical configuration.

	Value
Transmitting optics	
Laser power [mW]	300–400
Laser wavelengths [nm]	514 and 488
Beam spacing [mm]	60
Frequency shift [MHz]	40
Transmitter focal length [mm]	510
Receiving optics	
Scattering angle [°]	30
Receiver focal length [mm]	500

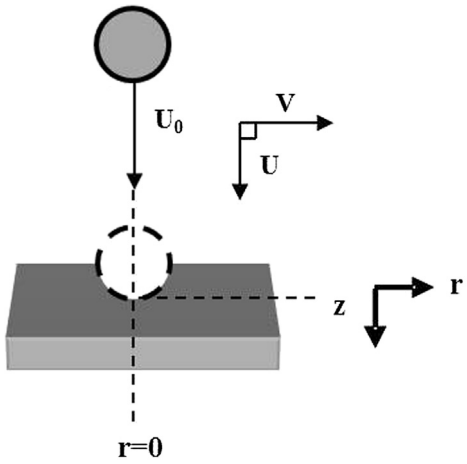

Fig. 2. Radial system of coordinates used in the measurements with the phase Doppler instrument.

Here, the temporal evolution of the spreading ratio, i.e. the spreading diameter made non-dimensional with the droplet's initial diameter $\beta(t) = d(t)/D_0$ is plotted for droplets impacting onto a non-heated smooth silicon wafer surface. The results can be interpreted by associating the concentration of the shear-thinning component to the fitting parameters of the constitutive models.

The η_0 value of the viscosity increases with growing mass fraction of the xanthan gum, as observed in Table 1. The higher concentrations slightly increase the power law index m, but mainly increase the consistency parameter K. Hence, following the arguments of German and Bertola [17], a dominant effect of the increase of the K factor is expected, which is associated to higher values of η_0. This is in line with the temporal evolution of the curves shown in Fig. 3. It is widely accepted that the deformation of a droplet can be divided in four main phases [20]: the kinematic phase, the spreading phase, the receding phase and the equilibrium phase. The kinematic phase takes place within the first instants after impact ($t < 1$ ms) and corresponds to the fast transfer of momentum and formation of the lamella in the radial direction. This phase is dominated by inertia. The spreading phase starts with the spreading of the liquid, from a truncated sphere in the radial direction, around the stagnation point located at the center (point of impact). At the beginning, the spreading phase is still dominated by inertia, but near the maximum spreading extent, capillarity forces and wetting effects become more important. Regarding the viscous dissipation, strong dissipation already occurs at the beginning of the spreading (for a dimensionless time $t^* = tD_0/U_0 < 2$) due to the large velocity gradients that occur within the lamella. These gradients will naturally be lessened as the liquid is decelerated at the end of the spreading phase, when the droplet attains its maximum diameter. Due to the excess of surface energy, after the maximum diameter is attained, the liquid recedes back to the core region, during the recoiling or receding phase, also dominated by capillarity and wettability effects. Subsequent spreading and recoiling motion can be observed until the droplet attains its equilibrium diameter. The detailed description of these stages has already been performed and can be found, for instance in Ref. [20]. The kinematic phase cannot be discussed in the results shown in Fig. 3, as the temporal resolution used is not

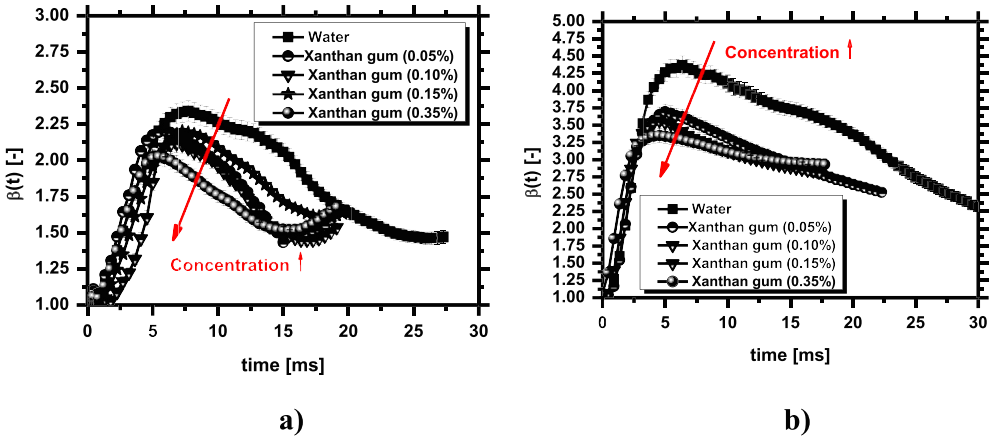

Fig. 3. Temporal evolution of the spreading rate of droplets of Newtonian (water, $D_0 = 3.2$ mm) and non-Newtonian (water + xanthan gum, $D_0 = 3.2$ mm) liquids, impacting on a non-heated and smooth silicon wafer surface, at: a) $U_0 = 0.8$ m/s and b) $U_0 = 2.0$ m/s.

short enough. Also, being solely governed by inertia, the influence of viscous effects is not worth to be discussed. Regarding the spreading phase, slightly faster expansion of the lamella is observed for the mixture with the largest concentration of the xanthan gum. This can be attributed to the high shear rate that leads the viscosity to get closer to η_∞ plateau. The rheological curves showed that for the mixtures used here, the η_0 is significantly larger for higher gum concentrations. The curves are not shown here, but also evidence a slightly higher slope in the decrease of the viscosity for higher shear rates, but at the end, the value of η_∞ is also larger for the mixtures with higher gum concentrations. This means that despite the flow may accelerate due to a faster decrease of the viscosity, it remains always more viscous for the mixtures with higher concentrations of the gum. These characteristics have two consequences: during the spreading phase, the viscous dissipation will be larger for the mixtures with higher gum concentration. Furthermore, as the shear rate quickly decreases, when the lamella approaches its maximum diameter and the liquid decelerates, the zero viscosity becomes quite large for higher concentrations of the gum. Consequently, the spreading diameter is smaller for the mixtures with higher gum concentration and a strong damping effect is observed during the receding stage. So, overall the maximum diameter is lower for increasing xanthan concentrations, but the equilibrium diameter overpasses that of the mixtures with lower xanthan concentrations (X0.05%) and gets closer to the equilibrium diameter of the water, for the latest stages of spreading (Fig. 3a). The limited recoiling phase is more evident for higher impact velocities, since although the shear rates at the beginning of the expansion of the lamella are larger, thus decreasing the viscosity (so the difference between the maximum diameters is not so accentuated), the dissipation associated to these large velocity gradients is actually higher (Fig. 3b), so the damping effect during the recoiling phase will be more noticeable. The acceleration during lamella expansion, due to shear-thinning effects is mild and therefore difficult to detect during the spreading period. However, one can notice it, since the time period required for the lamella to attain its maximum diameter is slightly smaller for larger concentrations. A more detailed investigation for data obtained with a higher temporal resolution is nevertheless required to deepen the description of this effect.

The spreading curve of water stands out from the shear-thinning mixtures, even for those with the lowest concentration. In the absence of shear-thinning effects, the spreading diameter of the water droplets is larger and its maximum value is consequently attained latter, when compared to the non-Newtonian droplets.

These results are consistent with those reported by German and Bertola [17] and by An and Lee [31,32]. The effect of the xanthan gum concentration (i.e. higher K and slightly higher m coefficients) is actually dominant when compared to other factors such as the surface wettability, as shown in Fig. 4. As aforementioned, significant effects of wettability are only noticed at the later stages of spreading (near the maximum diameter) and during recoiling, so they will be important only when low shear rates are present and therefore the viscosity of the mixtures is close to the η_0 plateau. The Figure shows that the influence of surface topography is quite less evident when compared to the previous results presented for Newtonian-droplets (*e.g.* Ref. [62]): a significant influence of the surface micro-patterning is only observed in the receding phase, for the cases in which the micro-patterning leads to a noteworthy modification of the wettability, quantified by the contact angle. This behaviour can be due to the aforementioned increase of the thickness of the lamella, resulting from the fact that at the later stages of spreading, the η_0 of the water + xanthan gum mixtures is larger than that of the water. Therefore, the ratio thickness of the lamella/amplitude of the rough pillars becomes smaller and the surface is "smoother" in relation to the new effective thickness of the lamella. This maybe so, since for the mixture with lower xanthan gum concentration, one may still observe some effect of the roughness: since the surfaces have a regular pattern, one may define the roughness ratio r_f=$[(2a + \lambda_R)^2 + 8ah_R]/(2a + \lambda_R)^2$. The roughness ratio relates the true to the wetted area. Since for all the surfaces used here, except for the superhydrophobic surface, a Wenzel or a non-stable Cassie-Baxter states estimated, larger r_f will in fact promote a larger wetted area, thus promoting both the dissipation at the contact line and possibly the viscous dissipation. Consistently, the spreading over the surfaces with larger r_f, is similar to that observed for the smooth surface, even though the contact angles are relatively high (the Wenzel state assures pinning of the contact line during spreading and therefore the liquid will definitely penetrate into the rough pillars). Only when the contact angle differs from 76° up to 154°, for the superhydrophobic surface, the dissipation at the contact line is lessened and allows a mild recoiling phase.

This trend is more evident for the mixture X0.35%. In this case, the lamella becomes thicker and is clearly insensitive to the roughness of the surface, so there is an evident recoiling phase only when the contact angle is near 100° and the dissipation at the contact line is lessened.

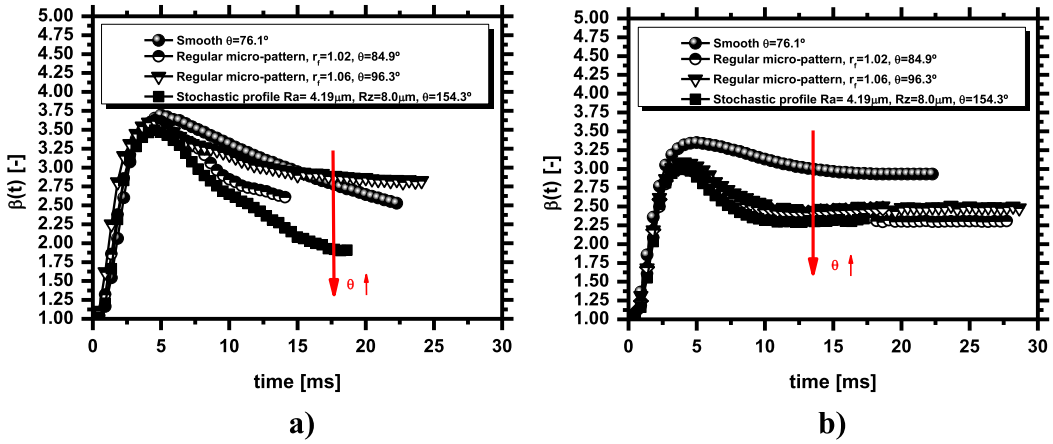

Fig. 4. Effect of surface wettability on the spreading behaviour of a 3.2 mm droplet impacting onto various non-heated surfaces at $U_0 = 2.0$ m/s: a) X0.05%, b) X0.35.

3.1.1. Influence of surface temperature ($T_{w,0} < T_{boiling}$)

The effect of surface temperature is not dominant, while the surface is heated bellow the liquid saturation temperature and the lamella does not boil. However, the results presented in Fig. 5 suggest that the heat transferred to the lamella alters the rheology of the mixtures and alters the viscosity plateaus, specially the zero viscosity.

This is particularly evident for the droplets of the mixtures with higher xanthan concentration, impacting the surface at larger velocity (i.e. when the shear-thinning nature is more pronounced), as shown in Fig. 5d: a lower spreading diameter is observed for droplet impacts at room temperature, which is followed by a very limited receding phase (as discussed in the previous paragraphs).

This behaviour contrasts to the relatively high value of β_{max}, obtained as the droplet hits the surface at $T_w = 100$ °C, which is followed by an evident receding phase. This effect cannot be related to evaporation of the water since when the water evaporates, the xanthan concentration would be higher, so the equilibrium diameter should be also larger, as discussed above. Hence, these results should be indeed attributed to rheological modifications of the mixtures. At this stage of the research it was not possible to perform a detailed characterization of the viscosity of the various mixtures

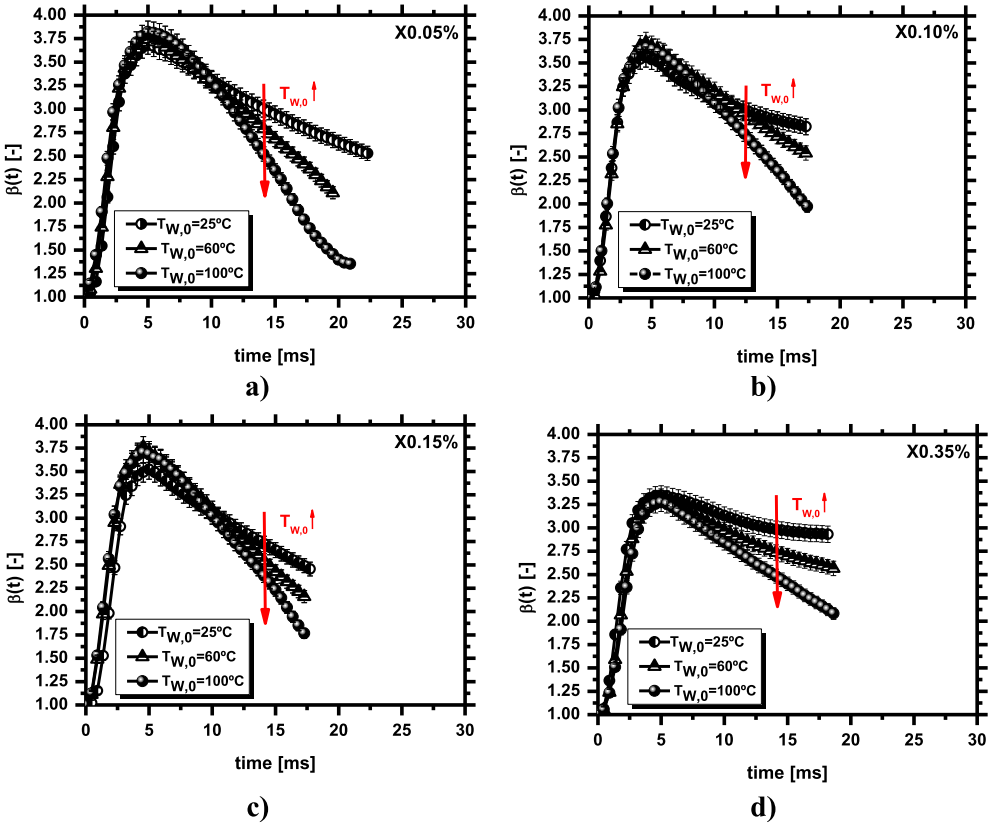

Fig. 5. Temporal evolution of the spreading rate of droplets ($D_0 = 3.2$ mm) of water + xanthan gum solutions, impacting on a smooth silicon surface heated at various temperatures, $T_{W,0} < T_{boiling}$. The droplets impact on the surface at $U_0 = 3.2$ m/s. a) X0.05%, b) X0.10%, c) X0.15%, d) X0.35%.

at different temperatures, to confirm this hypothesis. Such analysis will be presented in a future work.

Still, one may explain the observed results as follows: physically, the shear thinning is explained by the breakdown of the structure formed by the interacting particles in the mixture. Therefore, the heat transfer from the surface to the liquid during the spreading of the lamella may contribute to the breakdown of this structure. As discussed in the previous sub-section, the time scale associated to the heat transfer is smaller than that related to the spreading process, so important part of the heat transfer still occurs at later stages of spreading and at the recoiling phase, for which the low shear rates will correspond to the viscosity values close to η_0. For the droplets spreading over the non-heated surfaces, the value of η_0 is quite high for the higher concentrations of the gum, contributing to the viscous dissipation near the stage of maximum spreading and damping the recoiling phase. However, as the surface temperature increases and heats the fluid at the liquid–solid interface, promoting the breakdown of the structure formed by the interacting particles, it will facilitate the spreading by decreasing the zero viscosity plateau.

3.2. Theoretical prediction of the spreading diameter

Most contemporary semi-empirical models for the description of the spreading derive analytical expressions to predict the spreading diameter based on a simple energy conservation equation (neglecting variations of the potential energy):

$$E_{Ki} + E_{Si} = E_{Kf} + E_{Sf} + E_{diss} \tag{3}$$

being E_K and E_S the kinetic and surface energy, respectively and E_{diss} the energy dissipated by viscous effects. The subscripts i and f stand for the initial and final states, respectively. The final state (f) is usually taken at the position where the diameter of the lamella is at its maximum value and where E_{diss} and E_{Sf} can be easily determined [76]. Exception is made to a few authors such as Scheller and Bousfield [77] who considered an entirely empirical approach, without using energy conservation. Nevertheless, a force balance between inertial, viscous and surface tension forces is addressed.

Major differences between the various existing models lay in the assumptions regarding the shape of the lamella, the estimation of the viscous dissipation and the way to account for wettability effects. The energy dissipation term, can be determined by:

$$E_{diss} = \int_0^{t_2} \int_V \phi dV dt \approx \phi V t_2 \tag{4}$$

where $\phi = \mu(\partial U_i/\partial x_j + \partial U_j/\partial x_i)\partial U_i/\partial x_j$ is the dissipation function and t_2 is a known time period after impact, for which the effect of viscous dissipation is expected to be relevant. The viscous dissipation function is subsequently scaled based on different assumptions. For instance, Chandra and Avedisian [34] scale the viscous function with the impact velocity U_0 and with the thickness of the lamella h, which was determined by mass conservation, approximating the lamella to a flattened disk. Others, such as Pasandideh–Fard et al. [78] proposed to use the boundary layer thickness δ as a scaling length, claiming that an overestimation of the maximum spreading diameter is obtained when h is used in the scaling. Wettability effects can be explicitly accounted in the spreading diameter by introducing the contact angle in the term of the surface energy of the spreading droplet, being the discussion focused on weather is more appropriate to use the equilibrium angle θ, or the dynamic contact angle θ_d. From the phenomenological point of view, it is recognized that the dynamic angles are more representative although good results can be obtained using the static angle, due to the low velocity of the contact line at maximum extent conditions. The equilibrium contact angle is also often preferred, given the difficulty in attaining accurate measures of the dynamic contact angle. In the present paper, the dynamic contact angle is considered, which was evaluated during the post-processing procedures, while determining the spreading diameter from the recorded images. Concerning the shape of the lamella, most models take the lamella as a flattened disk with diameter $d(t)$ and height $h(t)$, so that relations between $d(t)$, $h(t)$ and D_0 can be easily determined by mass conservation. In this context, Roisman et al. [79] report the incapability of energy conservation-based models to describe the flow inside the droplet, due to this simplification of the shape of the lamella. These authors compared experimental data with numerical results for the shape of the lamella and found that its thickness for sufficiently high Reynolds ($\mathrm{Re} = \rho D_0 U_0/\mu$) and Weber ($\mathrm{We} = \rho D_0 U_0^2/\sigma_{lv}$) numbers (reminding that ρ, σ_{lv} and μ are the density, surface tension and dynamic viscosity of a Newtonian fluid) does not depend on liquid viscosity and surface tension. Hence, an approximation for the maximum spreading could be derived out of the kinematics. Hence, three different modes were considered to cover a wide range of possible cases in droplet impact, based on these two non-dimensional groups. In this context, Attané et al. [80] also discuss the limitations of considering the lamella approximated to a flattened disk, but at the end describe the wetting effects with the static contact angle and address the spreading lamella as a flattened disk, grounded on the argument that it is a good approximation because the viscous dissipation at the moment of impact is less relevant when compared to an adequate description of the spread factors larger than 1.

Given the various morphological similarities observed between the spreading of Newtonian and non-Newtonian droplets, a logical approach is to adapt the existing models to the non-Newtonian case, namely by integrating in the model the accurate constitutive models describing the viscous dissipation and making the adequate scaling. Following this approach one made an exhaustive review of the models and correlations predicting the spreading diameter of Newtonian droplets and compared them with our own experimental results. So, Fig. 6 confronts the models of [17,77–80] with our data obtained from impacts of a 3.2 mm droplet of distilled water over a smooth silicon wafer surface. These models were selected as they are illustrative of the various approaches and

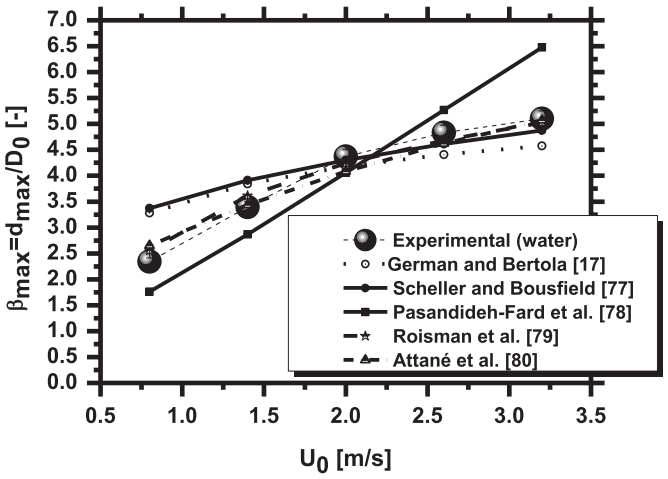

Fig. 6. Comparative analysis between various semi-empirical models for the prediction of the spreading diameter of Newtonian droplets impacting onto cold and rigid surfaces.

simplifications summarized in the previous paragraphs. It should be noticed that regarding the model of Attané et al. [80], only the equation associated to the so called free-spreading model was considered. Deviations between the experimental data (dots) and the theoretical predictions (lines) can be explained by several differences in the experimental conditions and particularly in the wettability and topography of the impacting surfaces, which can significantly affect the spreading diameter. However, the disagreement between experiments and theory is also due to the empirical nature of the correlations. Most of the models deviate from our experimental data between 20 and 40%, exception made to the model of Roisman [79] which deviates only 10%. One of the reasons for this better agreement may be the scaling, which considers different shapes of the lamella, resulting in different equations, depending on the relative importance of the inertia vs capillary and viscous terms. Such approach allows the model to follow well the trend of the maximum spreading diameter at both regions of low and high Weber numbers.

It is worth mentioning that despite the aforementioned limitations, these models already provide very satisfactory quantitative description of the spreading diameter of Newtonian droplets. Hence, the approach which resulted in the best correlation agreeing with the experimental spreading diameter, i.e. the model of Roisman [79] was modified to include the proper constitutive models describing the non-Newtonian behaviour of the spreading droplets. The resulting relation is evaluated by comparison with the experimental data presented in Section 3.1. Hence, the relation of Roisman [79] can generally be represented as:

$$\beta_{\max,\,\text{predicted}} = C_1\left(\text{Re}_{\text{eff}}^2\text{Oh}\right)^n \tag{5}$$

being $\text{Oh} = (\text{We})^{1/2}/\text{Re}$ the Ohnesorge number.

Scaling the viscous dissipation term with the boundary layer thickness δ, as suggested by An and Lee [32], an effective Reynolds number $\text{Re}_{\text{eff}} = U_0 D_0/\eta_{\text{eff}}$ can be defined with:

$$\eta_{\text{eff}} = \frac{\eta_0 - \eta_\infty}{1 + \left(C\cdot C_3 \cdot \frac{\sqrt{\frac{\rho U_0 D_0}{\eta_{\text{eff}}}}\cdot U}{2D_0}\right)^m} + \eta_\infty \tag{6}$$

In a different approach, one may also directly introduce the scaling of the lamella thickness h in the model, considering an effective viscosity, also based on the Cross model. The resulting modified formula is given by:

$$\beta_{\max,\,\text{predicted}} = C_1\left[\left[\frac{\rho U_0 D_0}{\frac{\eta_0-\eta_\infty}{1+\left(C\cdot C_3\cdot\frac{3\beta_{\max}^2\cdot U_0}{2D_0}\right)^m}+\eta_\infty}\right]^2\cdot\frac{\frac{\eta_0-\eta_\infty}{1+\left(C\cdot C_3\cdot\frac{3\beta_{\max}^2\cdot U_0}{2D_0}\right)^m}+\eta_\infty}{\sqrt{\rho D_0\sigma_{\text{lv}}}}\right]^n \tag{7}$$

Comparing the theoretical predictions with the experimental data, as depicted in Fig. 7 one may notice a slightly better agreement between the modified Roisman relation (eqs. (5)–(6)) for the spreading of the mixtures with lower concentration of the shear-thinning component (Fig. 7a). Regarding the largest spreading of the mixture with the largest concentration, shown in Fig. 7b, slightly better agreement is obtained for the experimental data when using the scaling based on the thickness of the lamella (eq. (7)) for the impacts at the lower velocities (lower Reynolds number), but a larger disagreement is obtained for the impacts at higher velocities.

These trends are probably related to the assumptions that are made. Hence, for lower impact velocities and higher xanthan concentrations, the effect of viscous and surface tension forces is more relevant and the non-Newtonian behaviour is more evident and strongly affects the thickness of the lamella, which is too high to be well represented by δ. Thus, for these conditions, the most adequate scaling is obtained directly using the thickness of the lamella h. Hence, the best solution is to use a different scaling, depending on the relative importance of the viscous dissipation effect, i.e. weather one is considering low or high Reynolds numbers, associated to the variation of the impact velocities and of the xanthan concentration. In line with these results, one proposes a combined solution with a different scaling, depending on the Re_{eff}. Hence, for lower values of $\text{Re}_{\text{eff}} < 580$ (Region I) the formulation used is given by eq. (7), while for $\text{Re}_{\text{eff}} > 3200$, (Region II) one recommends the use of eqs. (5)–(6) instead.

This combined solution is plotted in Fig. 8, together with the experimental results of An and Lee [31]. The agreement with the experimental data is rather good, within ±13% variation. The discrepancies observed for the results reported in the literature are also not evident, thus confirming the secondary role of the surface wettability for these experimental conditions, when dealing with the non-Newtonian mixtures. Largest variations are observed for impacts at lower velocity for which capillary effects are more important (*e.g.* Ref. [32]). Between these regions there is a transition zone, which is not well described yet and, therefore, the prediction line deviates more from the experimental data.

The relation proposed here is a first approach and therefore it is not yet independent from empirical fitting and therefore can be improved, particularly to predict more accurately the spreading behaviour of the droplets with larger concentration of the shear-thinning component, impacting the surface at higher velocities. However, it already predicts quite well (within 13%) all the experimental data, exception made to the so-called "transition area" Also, the effect of the surface temperature is not accounted yet, as further investigation is required to explain in detail the phenomena described in Section 3.1. Coupling the thermal analysis that is presented in the following section with the model of the spreading also requires more work. In parallel to this analytical approach, a numerical study is being performed, which will complement the first approach that is being discussed here. However, given the sparse information that still exists regarding the spreading of shear-thinning droplets, one finds relevant to present already this first attempt.

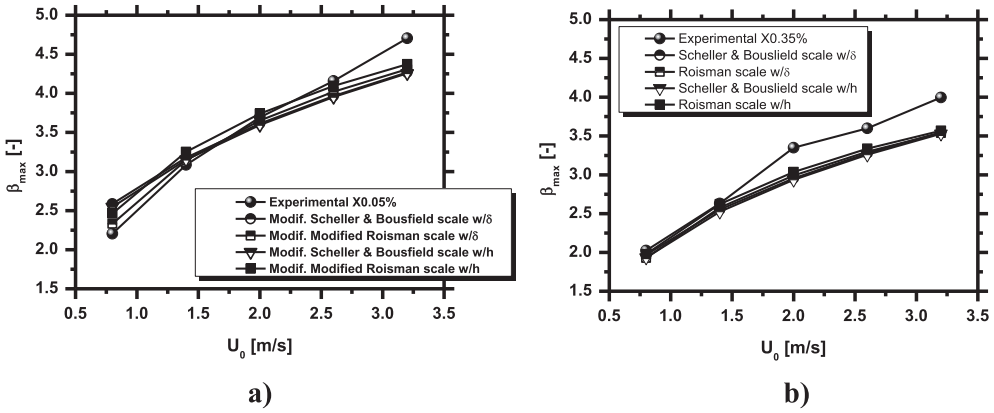

Fig. 7. Theoretical prediction of the maximum spreading diameter vs experimental data for: a) X0.05% solution, b) X0.35% solution.

3.3. Heat transfer processes during droplet–wall interactions

The temporal evolution of droplet impact can be related to the variation of the temperature measured by a fast response thermocouple, which is located at the impact point ($r = 0$ mm) and aligned to the top of the surface. Representative measurements are addressed in Fig. 9 for a water droplet, when the surface temperature is taken at two different values, one bellow saturation ($T_{sat}-T_{W,0} = 15$ °C) and the other slightly above saturation ($T_{W,0}-T_{sat} = 20$ °C) but still without the occurrence of thermal induced atomization.

The sudden temperature decrease after impact is mainly due to the heat transfer by sensitive heat from the surface, which can be as high as 30%. Despite this sudden decrease of the temperature at the contact point with the droplet, the bulk temperature of the liquid, is low and at the liquid–solid interface can be approximately estimated by the contact temperature T_c (*e.g.* Ref. [35]), obtained from the exact solution available for two semi-infinite solids: $T_c = T_{W,0}\cdot\varepsilon_W + T_l\cdot\varepsilon_l/\varepsilon_W + \varepsilon_l$, where ε_W and ε_l are the thermal effusivities of the surface and of the liquid, respectively, with $\varepsilon = (\rho k C_p)^{1/2}$, being ρ the density, k the thermal conductivity and C_p the specific heat, as early suggested by Seki et al. [44]. However, the temperature recover is rather slow and takes place during the period when the spreading is still occurring, for which the heat transfer continues and will affect the spreading process. Particularly, when the temperature is above saturation, phase transition is likely to occur, leading to an atomization process induced by thermal effects (which will be discussed in Section 3.4). As shown by several authors [35,47,54], the thermal properties of the fluid (and of the surface) play the major role in this process, so that these authors mainly determined substantial differences on the variation of the instantaneous temperature when changing the working fluid or altering the surface properties. Consistently, any significant changes were detected by using the various water + xanthan gum mixtures, as the thermal properties of the mixtures are very similar to those of the water. Since there is still no significant boiling of the spreading droplet, the temperature variation is similar for the impacts over the surface bellow or above T_{sat}, except for the larger temperature decay, which is naturally associated to the higher sensitive heat term. As shown in Refs. [62], when the lamella boils, the recovering of the surface temperature is even slower and strong temperature oscillations can be observed in the temperature profiles, which were attributed to the presence of vapour bubbles.

On the other hand, the overall heat that is transferred between the liquid and the surface is naturally dependent on the properties of the fluids, but is also affected by droplet dynamics, namely by the spreading area. This later effect is difficult to observe at an instantaneous analysis, but can be taken under a proper evaluation of the heat transferred during the spreading motion. Despite the valuable efforts made so far, which allowed significant progress in the modelling of the heat transfer at droplet–surface interactions, a

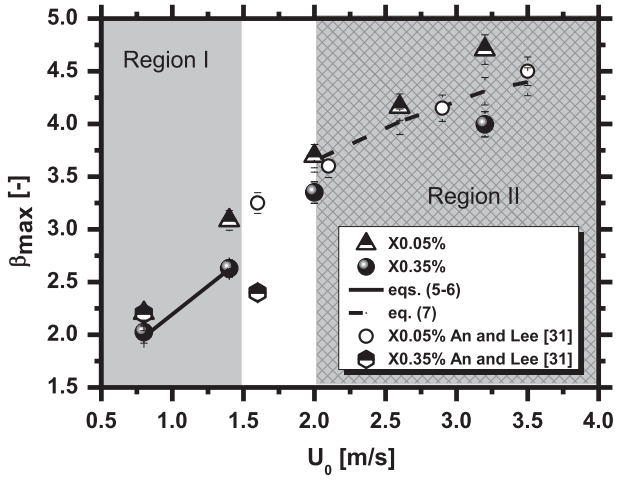

Fig. 8. Comparison between the theoretical prediction of the maximum spreading diameter and the experimental data.

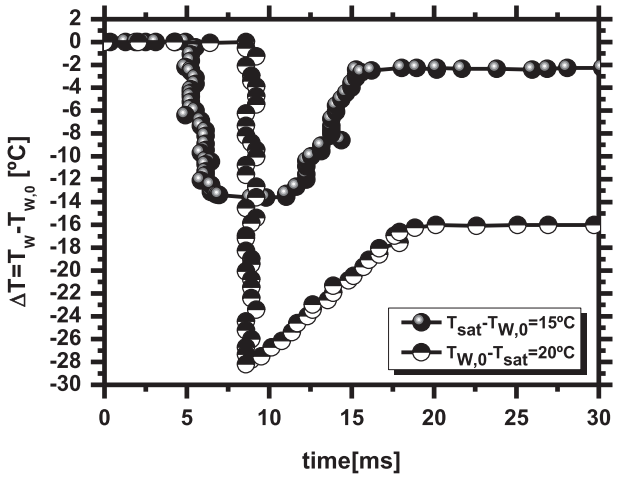

Fig. 9. Temporal evolution of the instantaneous surface temperature for a water droplet ($D_0 = 3.2$ mm) impacting on the smooth silicon wafer surface at different initial surface temperatures $T_{W,0}$.

full consensual description has not yet been achieved. For instance [54], proposed a new approach for the theoretical analysis of the flow and the temperature fields in a spreading droplet and in the solid substrate, based on a similarity solution of the Navier–Stokes equations, coupled with the energy equation. The solution, which is valid for the non-isothermal case, accounts for the variation of the thermal properties of the liquids with the temperature, which has been shown by Healy et al. [35] to be of major importance. The output of this model is basically a scaled gradient of the temperature right at the interface, $T_c^{'}$ obtained as the root of equation: $T_c^{'}(T_c) = \sqrt{\mu}\varepsilon_W/[\sqrt{\pi}k(T_c)]\cdot(T_c - T_{W,0})$ for known values of the surface effusivity of its initial temperature, $T_{w,0}$, and of the dependence of the liquid thermal conductivity on temperature. T_c is mainly the contact temperature as defined by Ref. [44].

Although this is an interesting approach, its validation is restricted to early times after impact, as aforementioned in the Introduction and, therefore it is not useful to explore the results coupled with the spreading of the non-Newtonian droplets, for which significant differences are mainly observed at later stages of spreading. Hence, it is better to address a simpler, although more appropriate approach, which takes into account the spreading process, at least up to the maximum spreading diameter. Such approach is based on the analysis reported by Pasandideh–Fard et al. [47] and was implemented as follows. The total heat transfer from the heated surface to the spreading drop can be estimated as:

$$q_c = \int_0^{t_c}\int_0^{A_{\max}} q^{''}\,dA\,dt \approx q^{''}A_{\max}t_c \tag{8}$$

where $A_{\max} = \pi d_{\max}^2/4$ is the maximum spreading area occurring at the corresponding instant t_c. The heat flux is given as:

$$q^{''} = k\frac{T_{w,0} - T_{d,0}}{\delta_T} \tag{9}$$

The thermal boundary layer thickness δ_T can be determined from a similarity solution for heat transfer for axisymmetric stagnation point flow (White [81]):

$$\delta_T = \frac{\delta}{\mathrm{Pr}^{0.4}} \tag{10}$$

where δ is the hydrodynamic boundary layer thickness which, according to White [81] and following the scaling performed in Pasandideh–Fard et al. [77] can be estimated as:

$$\delta = 2D_0\mathrm{Re}^{-0.5} \tag{11}$$

So, the heat flux during the spreading of the lamella can be estimated as:

$$q^{''} = k\frac{T_{w,0} - T_{d,0}}{2D_0}\mathrm{Re}^{0.5}\mathrm{Pr}^{0.4} \tag{12}$$

being $\mathrm{Pr} = Cp\mu/k$. the Prandtl number.

In the present work δ_T and δ are estimated as in Pasandideh–Fard et al. [47] (numerical calculations show that this is a good approximation for the conditions studied here) and $d_{\max}$ is taken from the dynamic analysis.

For the non-Newtonian cases, the hydrodynamic boundary layer was adjusted as in eqs. (5)–(7), so in this case the heat flux is given by eq. (12) with the required adjustments to include the effective Reynolds and Prandtl numbers. The most practical analysis should relate the heat transfer with the influencing parameters in a dimensionless form. Hence, following [47], one may define the cooling effectiveness as:

$$\zeta = \frac{\int_0^t\int_0^A q^{''}\,dA\,dt}{mC_p(T_{w0} - T_{d0})} \tag{13}$$

This quantity, computed for the experimental conditions addressed here, can be compared with the data reported in Refs. [47], for the Newtonian case (water droplets), as depicted in Fig. 10.

The results evidence a strong dependence of the cooling effectiveness with the Weber (Fig. 10a) and effective Reynolds (Fig. 10b) numbers for the non-Newtonian droplets. For illustrative purposes, only the extreme cases of largest and lowest gum concentrations are shown, for the impact of the droplets at different surface temperatures and for 3 distinct impact velocities.

The cooling effectiveness of the water droplets is not strongly dependent on the impact Weber and Reynolds numbers. One may argue that the cooling effectiveness is slightly larger for higher Weber and Reynolds, numbers, due to the increased spreading area. This trend however is much stronger in the non-Newtonian droplets, due to their shear thinning nature. Hence, the effective viscosity changes as the impact Weber and Reynolds number increase (as the spreading velocity and the shear rates will also increase), so the spreading diameter will vary more abruptly, when compared to the Newtonian droplets.

This will naturally lead to a significant increase of the wetted area and consequently of the cooling effectiveness. The overall lower effectiveness of the non-Newtonian droplets is related to the lower spreading diameter obtained for the non-Newtonian mixtures, but also to an overall higher Prandtl number, which is associated to the large momentum diffusivity, particularly for the mixtures with higher gum concentration. The slightly better cooling effectiveness obtained for the impacts over the surfaces with higher temperature T_W is due to the larger spreading diameter which, in turn is attributed to the decrease in the zero plateau viscosity caused by the liquid heating that promotes the breakdown of the structure formed by the interacting particles in the mixture, as previously discussed in Section 3.1.

This simple analysis also highlights the strong interdependence between the heat transfer process and the spreading dynamics, for the non-Newtonian droplets.

3.4. Droplet morphology for surface temperatures $T_w > T_{boiling}$: thermal induced atomization

Up to now, the surface temperature was kept low enough to prevent thermal induced atomization. Further heating the surface, up to $T_{W,0} = 140\ ^\circ\mathrm{C}$, the heat transfer regime falls fully within the nucleate boiling region. As explained in Section 3.1, the characteristic time scale of momentum transfer from the vertical to the horizontal direction and subsequent spreading of the droplet (of the order of micro to milliseconds) is much faster than that of heat transfer between the droplet and the surface (which takes tens of milliseconds). Consequently, only at later stages of spreading ($1 < t^* < 7$), when the amount of heat removed is high enough to cause phase transition, bubble explosions are triggered from the thinner part of the spreading film. As the spreading quickly progresses and the diameter tends to reach its maximum extent, the boiling intensifies giving rise to a spectrum of continuously growing bubbly structures from which secondary droplets are ejected later. This disintegration process, described in detail for instance in Refs. [66,71,82] is not governed by inertial forces (which overcome the surface tension forces, disrupting the lamella) but is

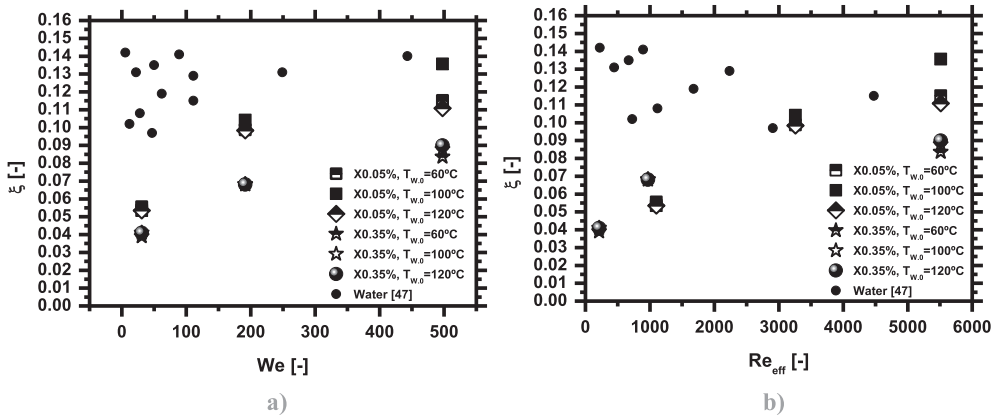

Fig. 10. Cooling effectiveness ξ related with the a) Weber number and with the b) (effective) Reynolds number.

solely generated by the heat transfer (sensitive and latent) processes. In Ref. [66] and in Ref. [71], Moita and Moreira quantified the ratio between the momentum of the incoming and of the ejected droplets, for various fluids, impacting over surface with different characteristics and showed that the higher momentum was associated to higher latent heat of vaporization and heat capacity of the fluids. They also report that the surfaces enhancing the heat transfer would also promote the thermal induced atomization to be triggered at earlier stages after impact, thus confirming the role of the heat transfer in this particular disintegration mechanism. Such detailed study was not yet performed for non-Newtonian droplets, but, visualization of droplet impacts, supported by combined image analysis and Phase Doppler measurements suggest that the secondary atomization is triggered mainly at the same time instant, regardless of the impact conditions and xanthan concentrations.

Only fewer droplets seem to be generated for higher concentrations of the xanthan gum, which can be associated to the fact that the higher concentration of the gum strongly decelerates the spreading of the droplet, thus thickening the lamella and consequently making more difficult to sustain the boiling process inside this thicker bulk.

Fig. 11 depicts the size distribution of the thermally induced secondary droplets, resulting from droplet impacts at different velocities, for three xanthan concentrations. As the concentration increases and consequently K and m parameters of the constitutive model are higher, large vapour bubbles are produced over the lamella and secondary atomization is mainly generated as they burst. The smaller number of secondary droplets associated to the difficulty in keeping the surface clean for these higher xanthan concentrations, makes the phase Doppler measurements very time consuming. Hence, measurements obtained for X0.35% are not presented here, as, up to now, they did not render reliable results. The figure evidences a very low dependence of the size of the secondary droplets with the shear-thinning effects associated to an increase of the concentration of the gum. A non-negligible effect is still noticed for the impacts at $U_0 = 1.2$ m/s, but for the highest impact velocity, the observed differences are within the measurement uncertainties.

These results suggest that the thermal induced atomization is not significantly dependent on the viscous dissipation, but instead is governed by the competition between surface tension and vapour forces, similarly to what occurs for the Newtonian droplets [66,71]. Therefore, only a mild effect of the viscosity is indeed expected to be observed in the size of the secondary droplets, which is only related to the fact that it is naturally scaled by the thickness of the lamella (*e.g.* Refs. [71,83]). At lower impact velocities, the higher concentrations of the gum are associated to the dominant effect of increasing the consistency parameter K, which is related to the increase of the zero viscosity plateau (η_0). Hence, as discussed in 3.1, the droplets with higher concentrations of the gum spread less so, by mass conservation, will have a thicker lamella. Consequently the ejected droplets are also slightly larger (Fig. 11a).

As the impact velocity is augmented, for Newtonian droplets, even though the thermal induced atomization is not governed by inertia, the inertial forces will lead to a wider spreading diameter and therefore, a thinner lamella, even for the non-Newtonian droplets. Given that the surface temperature tends to lessen the zero viscosity, the spreading behaviour of the droplets tends to be more uniform, so that the mild effect observed at lower impact velocities becomes negligible (Fig. 11b).

The (low) effect of the viscosity in the size of the secondary droplets can be at least partially captured by the Re_{eff}, which can be included in the correlations that are usually proposed to predict the size of the secondary droplets (*e.g.* Ref. [71]). However, a more detailed analysis is now required, over a wider range of experimental data, to confirm the observed behaviour and accurately describe it.

4. Final remarks

The study presented here focuses on the experimental and theoretical description of the fluid dynamic and thermal behaviour of non-Newtonian (shear-thinning) droplets impacting onto smooth, micro-patterned and heated surfaces. The shear-thinning liquids are mixtures of water + xanthan gum prepared with different concentrations of the gum, namely 0.05%, 0.10%, 0.15% and 0.35%wt.

When the droplet impacts over the surfaces heated bellow the boiling temperature of the liquid, the shear-thinning nature of the liquid is influencing the spreading and receding motion. Hence, the initial acceleration of the flow associated to an increased dissipation (higher values of zero viscosity) at the end of the spreading phase lead to a smaller diameter which occurs earlier for the mixtures with higher concentrations of the shear-thinning component. The strong increase of the zero viscosity also precludes the occurrence of the receding phase for the largest xanthan concentrations. This behaviour, which is governed by the concentration of the non-Newtonian component is well related to the consistency coefficient of the constitutive model, which describes the viscous behaviour of the flow. The results further suggest that heating the surface (and consequently the liquid) alters the rheology of the non-Newtonian mixture and reverses the increase

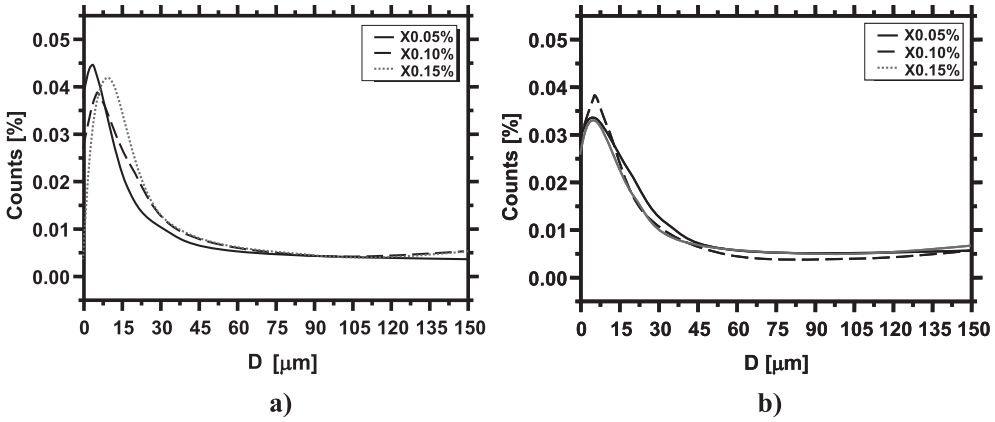

Fig. 11. Size distribution for the secondary droplets (measured by Phase Doppler Anemometry) resulting from the impact of 3 mm non-Newtonian droplets onto a smooth and heated silicon wafer surface ($T_{W,0}$ = 140 °C) for various Xanthan gum concentrations. a) U_0 = 1.4 m/s, b) U_0 = 3.2 m/s.

of the zero viscosity. In line with these trends, an alternative mode is proposed here, which includes the non-Newtonian behaviour of the spreading lamellas. A basic evaluation of the heat transferred at droplet–surface interaction, during the spreading of the droplet evidences the strong coupling between the heat transfer process and the spreading dynamics, for the non-Newtonian droplets. Due to their shear-thinning nature, the effective viscosity will change as the impact Weber and Reynolds number increase (as the spreading velocity and the shear rates will also increase), so the spreading diameter will vary more abruptly, when compared to the Newtonian droplets. This will naturally lead to a significant variation in the total heat transferred between the droplet and the surface and consequently to a noticeable variation of the so called cooling effectiveness, defined as the ratio between the heat transferred up to the maximum extent of the lamella and the total amount of heat that can theoretically be removed by the mass of the impacting droplet. Furthermore, there are also significant differences in the thickness of the hydrodynamic boundary layer identified in a large increase of the Prandtl number, particularly when the concentration of the gum increases. These variations of the Prandtl number should be well address in any modelling of the heat transfer process. This analysis also highlights that it is vital to accurately describe the spreading process of the non-Newtonian droplets in order to be able to model the heat transfer process.

When the surface is heated above the saturation temperature of the liquid, and the amount of heat removed is high enough to cause phase transition, bubble explosions are triggered from the spreading lamella, giving rise to a thermal induced secondary atomization of the primary impacting droplets. This mechanism is mainly triggered by the force balance between surface tension and vapour pressure forces, and the size of the secondary droplets is just slightly affected by the non-Newtonian viscous behaviour of the droplets: at small impact velocities, higher concentrations of the gum are associated to the dominant effect of increasing the consistency parameter K, which in turn is related to the increase of the zero viscosity plateau (η_0). Consequently, the higher concentrations, will lead to a thicker lamella, which generates slightly larger secondary droplets, as it disrupts.

Acknowledgements

The authors are grateful to Fundação para a Ciência e a Tecnologia (FCT) for partially financing the research under the framework of project RECI/EMS-SIS/0147/2012.

A.S. Moita also acknowledges the contribution of FCT for financing her Post-Doc Fellowship (Ref.:SFRH/BPD/63788/2009).

References

[1] W.J. Frith, P. d'Haene, R. Buscall, Shear thinning in model suspensions of sterically stabilized particles, J. Rheol. 40 (1996) 531–548.
[2] V. Bertola, M. Marengo, Single Drop Impacts of Complex Fluids: a Review, Koninklijke Brill NV, Leiden, 2012, pp. 267–298 (Chapter 11).
[3] E.C. Bingham, An investigation of the laws of plastic flow, U.S. Bur. Stand. Bull 13 (1916) 309–353.
[4] W.H. Herschel, R. Bulkley, Konsistenzmessungen von Gummi-Benzol-Lösungen, Kolloid Z 39 (1926) 291–300.
[5] T.C. Papanastasiou, Flows of materials with yield, J. Rheol. 31 (1987) 385–404.
[6] Q.D. Nguyen, D.V. Boger, Measuring the flow properties of yield stress fluids, Ann. Rev. Fluid. Mech. 24 (2007) 47–88.
[7] H.A. Barnes, The yield-stress – a review or 'παητα ρει' – everything flows? J. Newt. Fluid Mech. 81 (1999) 133–178.
[8] P. Coussot, Rheophysics of pastes: a review of microscopic modeling approaches, Soft Matter 3 (2007) 528–540.
[9] D.D. Joseph, Fluid Dynamics of Viscoelastic Liquids, Springer-Verlag, New York, Berlin, Heidelberg, 2002.
[10] H. Zhu, D. Kee, K. de Frederic, A constitutive model for flow induced anisotropic behaviour of viscoelastic complex fluids, J. Newt. Fluid Mech. 157 (2009) 108–116.
[11] H.S. Koo, M. Chen, P.C. Pan, L.T. Chou, F.M. Wu, S.J. Chang, T. Kawai, Fabrication and chromatic characteristics of the greenish LCD colour-filter layer with nano-particle ink using inkjet printing technique, Displays 27 (2006) 124–129.
[12] F.V. Lopez, A. Diez, A. Odriozola, Inkjet printing of conductive and resistive coatings, Int. Polym. Process 22 (1) (2007) 27–33.
[13] Y. Son, C. Kim, Spreading of inkjet droplet of non-Newtonian fluid on solid surface with controlled contact angle at low Weber and Reynolds numbers, J. Newt. Fluid Mech. 162 (2009) 78–87.
[14] K.J. Mysels, (1949) Flow thickened fluids, U.S. Patent 2,492,173, Dec. 27, 1949.
[15] A.B. Metzner, in: J.P. Hartnett, T.F. Irvine Jr. (Eds.), Heat Transfer in Non-Newtonian Fluids, Adv. Heat Transfer, vol. 2, Academic, New York, 1965, p. 357.
[16] S. Nigen, Experimental investigation of the impact of an (apparent) yield-stress material, Atom. Sprays 15 (2005) 103–117.
[17] G. German, V. Bertola, Impact of shear-thinning and yield-stress dropson solid surfaces, J. Phys. Condens. Matter 21 (2009) 375111.
[18] L. Luu, Y. Forterre, Drop impact of yield-stress fluids, J. Fluid Mech. 632 (2009) 301–327.
[19] A. Saidi, C. Martin, A. Magnin, Influence of yield-stress on the fluid droplet impact control, J. Newt. Fluid. Mech. 165 (2010) 596–606.
[20] R. Rioboo, M. Marengo, C. Tropea, Time evolution of liquid drop impact onto solid, dry surfaces, Exp. Fluids 33 (1) (2002) 112–124.
[21] S. Sikalo, M. Marengo, C. Tropea, E.N. Ganic, Analysis of impact of droplets on horizontal surfaces, Exp. Therm. Fluid Sci. 25 (7) (2002) 503–510.
[22] A. Saidi, C. Martin, A. Magnin, Effects of surface properties on the impact process of a yield-stress fluid drop, Exp. Fluids 51 (2011) 211–224.
[23] M. Vignes Adler, Physico-chemical aspects of forced wetting, in: Martin Rein (Ed.), Drop-surface Interactions, SpringerWien, NewYork, 2002, p. 103.
[24] A. Rozhkov, B. Prunet-Foch, M. Vignes-Adler, Impact of water on small targets, Phys. Fluids 14 (2002) 3485–3501.
[25] D. Bartolo, A. Boudaoud, G. Narcy, D. Bonn, Dynamics of non-Newtonian droplets, Phys. Rev. Lett. 99 (2007) 174502.

[26] T. Xu, J. Jin, A.C. Gregory, J.J. Hickman, T. Boland, Inkjet printing of viable mammalian cells, Biomaterials 26 (2006) 93–99.
[27] S. Tasoglu, G. Kaynak, A.J. Szeri, U. Demirci, M. Muradoglu, Impact of compound droplet on a flat surface: a model for single cell epitaxy, Phys. Fluids 22 (2010) 082013.
[28] A.B. Robins, Non-Newtonian behaviour of dilute DNA solutions, Trans. Faraday Soc. 60 (1964) 1344–1351.
[29] K. Sharma, S.V. Bhat, Non-Newtonian rheology of leukemic blood and plasma: are n and K parameters of power law model diagnostic? Phys. Chem. Phys. Med. NMR 24 (4) (1992) 307–312.
[30] M. Brust, C. Schaefer, R. Doerr, L. Pan, P.E. Arratia, C. Wagner, Rheology of human blood plasma: viscoelastic versus Newtonian behaviour, Phys. Rev. Lett. 110 (2013) 078305.
[31] S.M. An, S.Y. Lee, Observation of the spreading and receding behaviour of a shear-thinning liquid drop impacting on dry solid surfaces, Exp. Therm. Fluid Sci. 37 (2012) 37–45.
[32] S.M. An, S.Y. Lee, Maximum spreading of a shear-thinning liquid drop impacting on dry solid surfaces, Exp. Therm. Fluid Sci. 38 (2012) 140–148.
[33] J.D. Bernardin, I. Mudawar, The Leidenfrost point: experimental study and assessment of existing models, Trans. ASME 121 (1999) 894–903.
[34] S. Chandra, C.T. Avedisian, On the collision of a droplet with a solid surface, Proc. R. Soc. Lond. A 432 (1991) 13–41.
[35] W.M. Healy, J.G. Hartley, S.I. Abel-Kalik, On the validity of the adiabatic spreading assumption in droplet impact cooling, Int. J. Heat. Mass Transf. 44 (2001) 3869–3881.
[36] S.L. Manzello, J.C. Yang, On the collision dynamics of a water droplet containing an additive on a heated solid surface, Proc. R. Soc. Lond. A 458 (2002) 2417–2444.
[37] S.L. Manzello, J.C. Yang, An experimental study of high Weber number impact of methoxy-nonafluorobutane $C_4F_9OCH_3$ (HFE7100) and n-heptane droplets on a heated solid surface, Int. J. Heat. Mass Transf. 45 (2002) 3961–3971.
[38] L.H.J. Wachters, N.A.J. Westerling, The heat transfer from horizontal plate to sessile water drops in the spheroidal state, Chem. Eng. Sci. 21 (1966) 923–936.
[39] L.H.J. Wachters, N.A.J. Westerling, The heat transfer from a hot wall to impinging water drops in the spheroidal state, Chem. Eng. Sci. 21 (1966) 1047–1056.
[40] A. Karl, A. Frohn, Experimental investigation of interaction processes between droplets and hot walls, Phys. Fluids 12 (2000) 785–796.
[41] K. Makino, I. Michiyoshi, The behavior of a water droplet on heated surfaces, Int. J. Heat. Mass Transf. 27 (5) (1985) 781–791.
[42] M. Abu-Zaid, A. Atreya, Effect of Water on Piloted Ignition of Cellulosic Materials, NIST Rept., GCR-89–561, 1989.
[43] P. Tartarini, G. Lorenzini, M.R. Randi, Experimental study of water droplet boiling on hot, non porous surfaces, Heat. Mass Transf. 34 (1999) 437–447.
[44] M. Seki, H. Kawamura, K. Sanokawa, Transient temperature profile of a hot wall due to an impinging liquid droplet, J. Heat. Transf. 100 (1978) 167–169.
[45] V.G. Labeish, Thermodynamic study of a drop impact against a heated surface, Exp. Therm. Fluid Sci. 8 (1994) 181–184.
[46] J.C. Chen, K.K. Hsu, Heat transfer during liquid contact on superheated surfaces, J. Heat. Transf. 117 (1995) 693–697.
[47] M. Pasandideh-Fard, S.D. Aziz, S. Chandra, J. Mostaghimi, Cooling effectiveness of a water drop impinging on a hot surface, Int. J. Heat. Fluid Flow. 22 (2001) 201–210.
[48] R. Bhardwaj, J.P. Longtin, D. Attinger, Interfacial temperature measurements, high-speed visualization and finite-element simulations of droplet impact and evaporation on a solid surface, Int. J. Heat. Mass Transf. 53 (19) (2010) 3733–3744.
[49] G. Strotos, M. Aleksis, M. Gavaises, K. Nikas, N. Nikolopoulos, A. Theodorakakos, Non-dimensionalisation parameters for predicting the cooling effectiveness of droplets impinging on moderate temperature solid surfaces, Int. J. Therm. Sci. 50 (5) (2011) 698–711.
[50] M. Di Marzo, D. Evans, Dropwise evaporative cooling of high thermal conductivity materials, Int. J. Heat. Tech. 5 (1987) 126–136.
[51] M. Di Marzo, D. Evans, Evaporation of a water droplet deposited on a hot thermal conductivity surface, ASME J. Heat. Transf. 111 (1989) 210–213.
[52] M. Di Marzo, P. Tartarini, Y. Liao, D. Evans, H. Baum, Evaporative cooling due to a gently deposited droplet, Int. J. Heat. Mass Transf. 36 (17) (1993) 4133–4139.
[53] S. Chandra, M. Di Marzo, Y. Qiao, P. Tartarini, Effect of liquid-solid contact angle on droplet evaporation, Fire Saf. J. 27 (1996) 141–158.
[54] A.S. Moita, I.V. Roisman, A.L.N. Moreira, Heat transfer during drop impact onto a heated surface, in: Proceedings of the ASME International Heat Transfer Conference, IHTC – 14, Washighton DC, U.S.A, 2010.
[55] Y.Y. Yan, Y.Q. Zu, C.Q. Tian, N. Gao, Droplets on micro structured or patterned surfaces with different roughness parameters, in: Proc. 14th International Heat Transfer Conference, IHTC-14, Washington D.C., U.S.A, 2010.
[56] B. Bhushan, E.K. Her, Fabrication of superhydrophobic surface with high and low adhesion inspired from rose petal, Langmuir 26 (11) (2010) 8207–8217.
[57] W.J. Jeong, H. Yeong, S.Y. Hyun, M. Ambrosia, Dynamic behaviour of water droplets on solid surfaces with pillar-type nanostructures, Langmuir 28 (2012) 5360–5371.
[58] N. Gao, Y. Yan, Characterisation of surface wettability based on nanoparticles, Nanoscale 4 (7) (2012) 2202–2218.
[59] N. Gao, Y. Yan, X. Chen, D.J. Mee, Nanoparticle-induced morphology and hydrophilicity of structured surfaces, Langmuir 28 (33) (2012) 12256–12265.
[60] N. Gao, Y. Yan, X. Chen, D.J. Mee, Superhydrophobic surfaces with hierarchical structure, Mater. Lett. 65 (19–20) (2011) 2902–2905.
[61] C. Weickgenannt, Y. Zhang, A.N. Lembach, I.V. Roisman, T. Gambaryan-Roisman, A.L. Yarin, C. Tropea, Nonisothermal drop impact and evaporation on polymer nanofiber mats, Phys. Rev. E 83 (2011) 036305.
[62] A.S. Moita, A.L.N. Moreira, Scaling the effects of surface topography in the secondary atomization resulting from droplet/wall interactions, Exp. Fluids 52 (3) (2012) 679–695.
[63] V. Bertola, K. Sefiane, Controlling secondary atomization during drop impact on hot surfaces by polymer additives, Phys. Fluids 17 (2005) 108104.
[64] M.M. Cross, Rheology of non-Newtonian fluids: a new flow equation for pseudoplastic systems, J. Colloid Sci. 20 (1965) 417–437.
[65] R. Rioboo, C. Tropea, M. Marengo, Outcome from a drop impact on solid surfaces, Atom. Sprays 11 (2001) 155–165.
[66] A.S. Moita, A.L.N. Moreira, Drop impacts onto cold and heated rigid surfaces: morphological comparisons, disintegration limits and secondary atomization, Int. J. Heat. Fluid Flow. 20 (2007) 735–752.
[67] A.L.N. Moreira, A.S. Moita, M.R. Panão, Advances and challenges in explaining fuel spray impingement: how much of single droplet impact research is useful? Prog. Energy Combust. Sci. 36 (2010) 554–580.
[68] B. Bhushan, Y.C. Jung, Natural and biomimetic artificial surfaces for superhydrophobicity, self-cleaning, low adhesion and drag reduction, Prog. Mater. Sci. 56 (2011) 1–108.
[69] R.R. Dreisbach, Applicability of the Eykman equation – an investigation using the best modern data, Ind. Eng. Chem. 40 (12) (1948) 2269–2271.
[70] G. Pitcher, G. Wigley, Sensitivity of drop size measurements by phase Doppler anemometry to refractive index changes in combusting fuel sprays, in: R.J. Adrian, D.F.G. Durão, F. Durst, M. Maeda, J.H. Whitelaw (Eds.), Proc. of the 5th Int. Symp. of Applications of Laser Techniques to Fluid Mechanics, Lisbon, Portugal, 1990, Springer-Verlag Berlin, Heidelberg, Germany, 1991.
[71] A.S. Moita, A.L.N. Moreira, Development of empirical correlations to predict the secondary droplet size of impacting boiling droplets, Exp. Fluids 47 (2009) 755–768.
[72] K.C. Basavaraju, T. Demappa, S.K. Rai, Miscibility studies of polysaccharide xanthan gum and PEO (polyethylene oxide) in dilute solution, Carbohydr. Polym. 69 (3) (2007) 462–466.
[73] M.R.O. Panão, Assessment of measurement efficiency in laser and phase-Doppler techniques: an information theory approach, Meas. Sci. Tech. 23 (12) (2012) 125304.
[74] M.R.O. Panão, A.L.N. Moreira, A real-time assessment of measurement uncertainty in the experimental characterization of sprays, Meas. Sci. Tech. 19 (9) (2008) 095402.
[75] R.B. Abernethy, R.P. Benedict, R.B. Dowdell, ASME measurement uncertainty, J. Fluids Eng. 107 (2) (1985) 161–164.
[76] A.S. Moita, A.L.N. Moreira, Droplet impact on a solid surface, in: Nasser Ashgriz (Ed.), Handbook of Atomization and Sprays: Theory and Applications, Springer, 2011 (Chapter 8).
[77] B.L. Scheller, D.W. Bousfield, Newtonian drop impact with a solid surface, AIChe J. 41 (6) (1997) 1357–1367.
[78] M. Pasandideh-Fard, Y.M. Qiao, S. Chandra, J. Mostaghimi, Capillary effects during droplet impact on a solid surface, Phys. Fluids 8 (3) (1996) 650–658.
[79] I.V. Roisman, E. Berberovic, C. Tropea, Inertia dominated drop collisions I. On the universal flow in the lamella, Phys. Fluids 21 (5) (2009) 052103.
[80] P. Attané, F. Girard, V. Morin, An energy balance approach of the dynamics of drop impact on a solid surface, Phys. Fluids 19 (1) (2007) 012101.
[81] F.M. White, Viscous Fluid Flow, second ed., McGraw-Hill, New York, 1991.
[82] G.E. Cossali, M. Marengo, M. Santini, Secondary atomization produced by single drop vertical impacts onto heated surfaces, Exp. Therm. Fluid Sci. 29 (2005) 937–946.
[83] I.V. Roisman, K. Horvat, C. Tropea, Spray impact: rim transverse instability initiating fingering and splash: description of a secondary spray, Phys. Fluids 18 (2006) 102104.